

CONFERENCES AND SYMPOSIA PACS number: 01.10.Fv

Joint scientific session of the Physical Sciences Division of the Russian Academy of Sciences and the Joint Physical Society of the Russian Federation (honoring the 110th birthday of P L Kapitza and the 70th anniversary of the P L Kapitza Institute for Physical Problems) (16 June 2004)

On 16 June 2004, a joint scientific session of the Physical Sciences Division of the Russian Academy of Sciences and the Joint Physical Society of the Russian Federation was held in the Conference Hall of the P L Kapitza Institute for Physical Problems, Russian Academy of Sciences, to honor the 110th birthday of P L Kapitza and the 70th anniversary of the host institute. The following reports were presented at the session:

(1) **Andreev A F** (P L Kapitza Institute for Physical Problems, RAS, Moscow) "Quantum crystals";

(2) **Dmitriev V V** (P L Kapitza Institute for Physical Problems, RAS, Moscow) "Spin superfluidity in ^{3}He";

(3) **Lebedev V V** (L D Landau Institute of Solid State Physics, RAS, Chernogolovka, Moscow Region) "Theory of weak crystallization";

(4) **Sosin S S, Prozorova L A, Smirnov A I** (P L Kapitza Institute for Physical Problems, RAS, Moscow) "New magnetic states in crystals".

Abridged versions of reports 2 and 4 are given below.

PACS numbers: **67.57.–z**, 67.57.Lm
DOI: 10.1070/PU2005v048n01ABEH001904

Spin superfluidity in ^{3}He

V V Dmitriev

1. Introduction

The hallmark of a superfluid liquid is its ability to assume quantum coherence, a state with a special kind of long-range order. The key characteristic describing this order in superfluid ^{4}He or common superconductors is a complex wave function, the so-called condensate wave function $\Psi = |\Psi| \exp(i\varphi)$ with a definite phase φ. This implies that the gauge invariance of the system breaks down at the superfluid transition. While the energy of superfluid liquid does not depend on the phase, it increases if φ becomes spatially nonuniform (i.e., when the so-called order parameter gradient energy increases). This gives rise to the mass- and (in superconductors) charge-carrying superfluid current

$$J_S = \frac{\hbar}{m} |\Psi|^2 \nabla\varphi = \rho_S v_S \,, \qquad (1)$$

where m is the mass of the ^{4}He atom and $\rho_S = |\Psi|^2$ and $v_S = (\hbar/m)\nabla\varphi$ are the superfluid component density and velocity, respectively. A constant phase difference $\Delta\varphi$ maintained between the ends of a channel filled with superfluid ^{4}He will give rise to a nondissipative current through the channel, whose magnitude will be proportional to this phase difference rather than the pressure or chemical potential difference as in a normal liquid. Correspondingly, electrical current in a superconductor is determined by the wave function phase difference between the electrons at the ends of the sample rather than by the voltage, as in a common conductor. The gradient energy can be viewed as kinetic energy associated with the superfluid current, $F_V = \rho_S v_S^2/2$, and the current is correspondingly written as $J_S = \partial F_V/\partial v_S$.

Unlike the atoms of ^{4}He, the atoms of ^{3}He are fermions, implying that their superfluidity results from Cooper pairing (analogous to superconductivity in metals). What is essentially new compared to common superconductors is that the spin and orbital moments of ^{3}He Cooper pairs are 1. Accordingly, there are three possible values for the projection of both the spin and the orbital moment on a chosen direction, and the order parameter is conveniently taken in the form of a complex 3×3 matrix which describes, in particular, how the spin and orbital moments of a Cooper pair are oriented with respect to one another (for more details on superfluid ^{3}He, see Refs [1 – 3]). Such ordering may correspond to various superfluid phases differing in the specific form of this matrix. In superfluid ^{3}He, only three phases — ^{3}He-A, ^{3}He-A$_1$, and ^{3}He-B — are found, depending on conditions (Fig. 1). In these phases, symmetries other than the gauge symmetry can also be violated. In particular, the violation of spin rotation symmetry in Cooper pairs leads to three additional hydrodynamic variables similar to the order parameter phase. The gradients of these variables will give rise to a spin supercurrent, a current in which spin and the related magnetic moment are transferred in a non-dissipative way (we do not distinguish between spin and magnetic currents below). It should be noted that what is meant by a spin supercurrent is magnetization transferred in the absence of mass transfer, not the flow of magnetized material. In general, the spin supercurrent is a tensor and can be written as

$$J_{kv} = \frac{\hbar}{2m} \rho_{ikv\sigma} \Omega_{i\sigma} \,, \qquad (2)$$

where $\rho_{ikv\sigma}$, the tensor of the superfluid spin density, is on the order of $\chi c^2/g$; c is a factor in the expression for the gradient energy and has the meaning of spin wave velocity; χ is the

Uspekhi Fizicheskikh Nauk **175** (1) 85 – 99 (2005)
Translated by E G Strel'chenko; edited by M V Magnitskaya

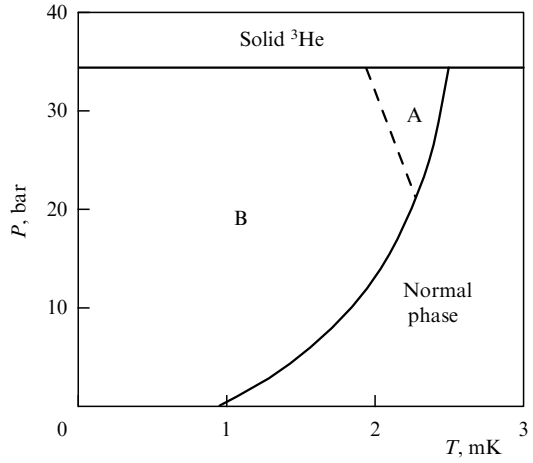

Figure 1. Phase diagram of ^{3}He in zero magnetic field. The A_1-phase occurs only in a magnetic field in a narrow region around the superfluid transition temperature.

magnetic susceptibility; g the gyromagnetic ratio; and $\Omega_{i\sigma}$ is a tensor characterizing the non-uniformity in spin space orientation. i and k are coordinate space indices, and v and σ are spin space indices.

The following reasoning leads to a simple model of how a spin supercurrent appears. In the momentum representation the wave function of a spin-1 Cooper pair can be expanded in components corresponding to various values of the projection of the Cooper pair spin ($m_s = 1, 0, -1$) onto a chosen direction, giving

$$\Psi = \Psi_{\uparrow\uparrow}|1,1\rangle + \Psi_{\downarrow\downarrow}|1,-1\rangle + \frac{1}{\sqrt{2}}(\Psi_{\uparrow\downarrow} + \Psi_{\downarrow\uparrow})|1,0\rangle\,, \quad (3)$$

where the $|1, m_s\rangle$ are the eigenfunctions of the spin operator projection. Now consider superfluid ^{3}He as consisting of a normal component and three superfluid components with wave functions $\Psi_{\uparrow\uparrow}$, $\Psi_{\downarrow\downarrow}$, and $(\Psi_{\uparrow\downarrow} + \Psi_{\downarrow\uparrow})$. Because in weak magnetic fields $|\Psi_{\uparrow\uparrow}| = |\Psi_{\downarrow\downarrow}|$, the counterflow of $\Psi_{\uparrow\uparrow}$ and $\Psi_{\downarrow\downarrow}$ should lead to superfluid spin transfer in the absence of mass transfer.

The possibility of a spin supercurrent began to be widely discussed immediately after the 1972 discovery of superfluidity in ^{3}He [4], when it became clear that the Cooper pairs of the new superfluid phases have a spin. However, direct evidence for the existence of such currents was lacking for a long time, leaving it unclear precisely which of the observable phenomena are caused by spin supercurrents and under what conditions these phenomena can be observed. The experiments A S Borovik-Romanov and his team started at the P L Kapitza Institute for Physical Problems in 1984 and theoretical work by I A Fomin of the L D Landau Institute of Theoretical Physics provided elucidation of the problem. In the present paper, a brief review of these studies is given. The experiments described in Section 4–7 were conducted at pressures from 0 to 29.3 bar in magnetic fields from 71 to 570 Oe [the corresponding nuclear magnetic resonance (NMR) frequencies ranging from 230 kHz to 1.85 MHz]. The problem of magnetic superfluidity can also be found in the review papers [5–8].

2. Spin supercurrent in ^{3}He-B

The violation of the spin space rotation symmetry in superfluid ^{3}He does not yet mean that spin supercurrent is easy to create and measure there. Unlike mass or electric charge, spin is not generally a conserved quantity. For example, the spin-orbit (dipole) interaction can lead to spin transfer to other degrees of freedom, and spin supercurrents can be considered meaningfully only if their effect is noticeable compared to spin-non-conserving processes. In superfluid ^{3}He spin-orbit interaction can be important because it is stronger than in the normal phase (due to the fact that Cooper pairs have a spin and an orbital moment). For this reason, talking about spin supercurrents only makes sense with respect to the B-phase, in which the spin-orbit interaction can be effectively eliminated. Therefore, the discussion below is limited to the B-phase.

The order parameter of the B-phase has the form

$$A_{vi} = \Delta \exp(\mathrm{i}\varphi)\hat{R}_{vi}(\hat{\mathbf{n}}, \theta) = \Delta \exp(\mathrm{i}\varphi)\hat{R}_{vi}(\alpha, \beta, \gamma)\,, \quad (4)$$

where Δ is the energy gap in the excitation spectrum and φ is the phase of the orbital part of the order parameter (a gradient of φ produces a mass supercurrent). The matrix $\hat{R}(\hat{\mathbf{n}}, \theta)$ of size 3×3 rotates the spin space with respect to the orbital space through an angle θ about the direction $\hat{\mathbf{n}}$ (which is common for a macroscopic volume of ^{3}He). Another way to express this rotation is in terms of the Euler angles α, β, and γ. The angle θ can in principle take on any value. In equilibrium, this degeneracy is lifted by imposing a minimum condition on the dipole energy

$$F_D = \frac{8}{15}\frac{\chi}{g^2}\,\Omega_B^2\left(\frac{1}{4} + \cos\theta\right)^2, \quad (5)$$

where $\Omega_B = \Omega_B(T)$, the so-called Leggett frequency, is a temperature-dependent characteristic of the dipole interaction force [$\Omega_B(0) \sim 200$ kHz]. The minimum of the dipole energy is achieved at

$$\theta = \theta_0 = \arccos\left(-\frac{1}{4}\right) \approx 104^\circ\,.$$

To excite a spin supercurrent, NMR experiments can be used. In an NMR experiment the spin part of the order parameter is in motion, the angles α, β, and γ depend on time, and the first two of them have a simple physical meaning: α corresponds to the phase of the magnetization precession, and β to the magnetization deviation angle from the equilibrium direction. The contributions due to the gradients of these angles lead to an increase in the spin gradient energy and hence produce a spin supercurrent.

In the spatially uniform case the spin dynamics of ^{3}He-B is determined by the Leggett – Takagi equations [9, 10]

$$\begin{aligned}
\dot{\mathbf{M}} &= g\mathbf{M}\times\mathbf{H} + \frac{4}{15}\frac{\chi\Omega_B^2}{g}\sin\theta\,(1+4\cos\theta)\hat{\mathbf{n}}\,,\\
\dot{\theta} &= g\hat{\mathbf{n}}\cdot\left(\frac{\mathbf{M}}{\chi} - \mathbf{H}\right) + \frac{4}{15\tau}\sin\theta\,(1+4\cos\theta)\,, \quad (6)\\
\dot{\hat{\mathbf{n}}} &= -\frac{g}{2}\left\{\hat{\mathbf{n}}\times\left(\frac{\mathbf{M}}{\chi} - \mathbf{H}\right) + \cot\frac{\theta}{2}\left[\hat{\mathbf{n}}\times\left[\hat{\mathbf{n}}\times\left(\frac{\mathbf{M}}{\chi} - \mathbf{H}\right)\right]\right]\right\},
\end{aligned}$$

where τ is the Leggett – Takagi effective time determining the magnetic relaxation rate. There are a number of NMR modes (i.e., of periodic magnetization motions) that follow from Eqn (6), of which the easiest to excite is the so-called Brinkman – Smith mode [11], that is the precession of magnetization deviated by an angle $\beta < \theta_0$ from the direction

of **H** (with $|\mathbf{M}| = \chi H$). What is remarkable about this mode is that $\theta = \theta_0$, i.e., the dipole energy remains zero during this precession. As a result, the last term on the right-hand side of the first equation of system (6) also goes to zero, as does the relaxation term in the second equation. Note that both the magnetization and the vector $\hat{\mathbf{n}}$ precess at the Larmor frequency (the orientation of $\hat{\mathbf{n}}$ relative to **M** is determined by precisely the condition that the dipole energy be a minimum). Let the magnetic field **H** be along the z axis and suppose that the system is homogeneous in the plane x, y but has inhomogeneities along the z-axis. Then, allowing for spin currents, the first equation of system (6) can be rewritten in the form

$$\dot{M}_v = (g\mathbf{M} \times \mathbf{H})_v + \frac{\partial J_{zv}}{\partial z}\,, \tag{7}$$

where v indexes the magnetization and current components (x, y, and z). For M_z, the first term on the right-hand side of Eqn (7) is zero, thus yielding the magnetization equation of continuity. If we transform to a Larmor-frequency-rotating coordinate system, this equation is also fulfilled for M_x and M_y, which is exactly what enables effects related to the spin supercurrent to be observed.

Given the minimum condition for the dipole energy, two of the three Euler angles (for example, α and β) can be chosen as independent, and in terms of the gradients of these two it is possible to obtain formulas for the spin supercurrent [12, 13]. For example, the spin supercurrent carrying the z-component of the magnetization in the direction of the z-axis is found to be

$$J_{zz} = -\frac{\chi}{g}\, c^2 \sqrt{1-u}\left[f_1(u)\, \frac{\partial \alpha}{\partial z} + f_2(u)\, \frac{\partial \beta}{\partial z} \right], \tag{8}$$

where $u = \cos\beta$,

$$f_1(u) = (2+u)\sqrt{1-u}\,, \qquad f_2(u) = \sqrt{\frac{3}{(1+4u)(1+u)}}\,.$$

From Eqn (8) it is seen that the analog of superfluid density in spin superfluidity is a quantity proportional to $\sqrt{1-u}$. Therefore, superfluid spin density is different from zero only for $\beta \neq 0$.

If the angle $\beta > \theta_0$, the dipole energy is minimum — but already not zero — at $\theta = \beta$, which results in a positive shift in the NMR frequency [11],

$$\omega - \omega_{\mathrm{L}} = -\frac{4}{15}\,\frac{\Omega_{\mathrm{B}}^2}{\omega_{\mathrm{L}}}\,(1 + 4\cos\beta)\,, \tag{9}$$

where ω and $\omega_{\mathrm{L}} = gH$ are the precession and Larmor frequencies, respectively. Note that the dipole moment on the right-hand side of the first equation of system (6) (and the relaxation term in the second) are also nonzero. Fortunately, under the conditions of the experiments to be described in Sections 3–7, these additional terms are small, and their associated non-conservation of spin affects spin dynamics little compared to magnetization transfer by spin currents.

3. A homogeneously precessing domain

There is an important consequence of the fact that ^{3}He-B can carry a spin supercurrent: the formation of the so-called homogeneously precessing domain (HPD). Let us see how an HPD forms under pulsed NMR conditions (Fig. 2). Let a

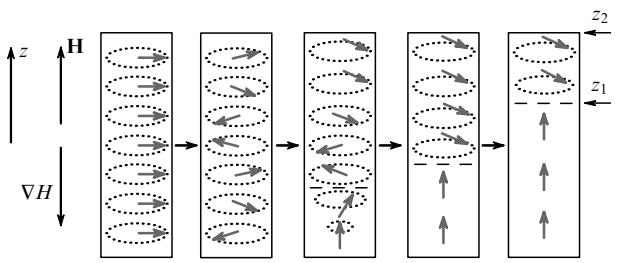

Figure 2. Formation of an HPD after the application of a deflecting rf pulse.

sample of ^{3}He-B be placed in a closed cell and exposed to a uniform magnetic field gradient. At equilibrium the magnetization is parallel to the field. Now let us apply a short rf pulse to get the magnetization deflected through a certain angle (90° in Fig. 2) throughout the volume. Then the magnetization in the volume enters the Brinkman–Smith mode, i.e., starts precessing at the Larmor frequency — which is coordinate dependent $[\omega_{\mathrm{L}}(z) = \omega_{\mathrm{L}}(0) - zg\nabla H]$ because the magnetic field varies along the cell — and the phase of the precession develops a gradient which increases with time. As the magnetization precesses, it produces an induction signal in the NMR pickup coil, for which, in a system of non-interacting spins, the decay time due to dephasing must be $T_2^* \sim 1/\Delta\omega = 1/(gL\nabla H)$, where $\Delta\omega$ is the characteristic precession frequency range over the cell and L the cell length. A different picture arises for ^{3}He-B. According to Eqn (8), a gradient in precession frequency leads to a spin supercurrent, which transports the longitudinal magnetization along the field gradient direction. Because there is no spin flow through the cell boundaries, the longitudinal component of the magnetization starts changing: the magnetic moment flows down to the bottom of the cell (here, M_z increases) and away from its top (here, M_z decreases). Since the absolute value of **M** in the Brinkman–Smith mode cannot change — this would lead to an increase in the dipole energy — what the change in the longitudinal magnetization does is to cause a change in the deviation angle β, upwards at the top and downwards at the bottom of the cell. This can continue until $0 < \beta < \theta_0$. At $\beta = 0$ we have the condition $J_{zz} = 0$, meaning that magnetization ceases to be transported in this region. As the angle β increases above $\theta_0 \approx 104°$, the dipole energy increases, and the precession frequency shifts from the Larmor value [see Eqn (9)]. This frequency shift can in principle (and does in practice) compensate for the nonuniform field and turn $\partial\alpha/\partial z$ and J_{zz} to zero. Accordingly, regions with $J_{zz} = 0$ appear and grow at the ends of the cell (a $\beta = 0$ region at the lower end and a $\beta \gtrsim \theta_0$ region at the upper end) to ultimately occupy the entire volume of the cell and form the so-called two-domain structure, where spin supercurrents are zero [13]. The lower domain is in fact unperturbed ^{3}He-B (a static domain, SD), whereas in the upper so-called homogeneously precessing domain the magnetization deviates by slightly more than θ_0 and precesses. This angle excess $\delta\beta = \beta - \theta_0$ depends on z in such a way that the resulting frequency shift compensates for the nonuniform field (nonuniform Larmor frequency) and the precession phase is the same throughout the sample, whereas the precession frequency is equal to the Larmor value $\omega_{\mathrm{L}}(z_1)$, where z_1 indicates the location of the interdomain wall. Under realistic experimental conditions ($H \sim 100$ Oe, $\nabla H_z \sim 1$ Oe cm^{-1}, $L \sim 0.5$ cm), $\delta\beta \sim 1°$, and the produced

dipole moment is sufficiently small, suggesting that the dynamics of the magnetization remain to be largely determined by the spin supercurrents: nonuniformities in the HPD lead to currents which cause the system to precess uniformly as before.

The interdomain wall has a characteristic thickness $\lambda = [c^2/(\omega\nabla\omega)]^{(1/3)} \sim 0.5$ mm. The angle β in the wall changes smoothly from $\sim 104^\circ$ to zero. In addition, the angle α changes by about 60°. Exactly how α and β change is determined by two conditions: first, the spin current in the wall due to inhomogeneities in β is compensated by the current due to inhomogeneities in α; and second, the precession frequency in the wall equals that of the entire HPD (because $\beta < \theta_0$ in the wall, the small frequency shift which is needed is ensured by the gradient energy [13]).

Magnetic relaxation in the two-domain structure proceeds by spin diffusion in the interdomain wall and by the Leggett – Takagi mechanism [10] in the bulk of the HPD, where there is a small shift from the local Larmor frequency [13]. This does not destroy the structure, however, and only leads to a smooth decrease in the size of the HPD and to an increase in the SD. As a result, the characteristic HPD lifetime is 0.1 – 1.0 s, much longer than the dephasing time of non-interacting spins. To summarize, a two-domain structure leads to an anomalously long-lived induction signal (LLIS). During the relaxation process the interdomain wall moves toward lower Larmor frequencies, therefore the frequency of the LLIS must fall off smoothly to $\omega = \omega_L(z_2)$.

4. A homogeneously precessing domain under pulsed NMR conditions (experiment)

The existence of LLIS in ^{3}He-B was first observed in Refs [14, 15], but the use of non-closed cells and the small amplitude of the LLIS made these experiments difficult to interpret. In our work [16, 17], virtually closed cells were used. The observed LLISs had large amplitudes and their frequencies were varied with time in a good agreement with the model in Section 3. Figure 3 is a schematic of the cell we used to directly prove the existence of an HPD. We placed a sample of ^{3}He-B in a cylinder aligned along the external magnetic field and used special gradient coils to apply a controlled magnetic field gradient to the sample. The magnetization was excited into free precession by applying a resonant rf pulse to the exciting NMR coil *1* (see Fig. 3). The induction signal was detected by two miniature pickup coils *2* and *3* located close to the opposite ends of the experimental volume; the sensitivity ranges of the coils did not overlap. Figure 4 exemplifies the time dependences of the induction signal amplitude recorded from both coils for the magnetic field gradient directed as in Fig. 3. The difference in the signals from coils *2* and *3* is explained as follows. Following the application of the rf pulse it takes about 10 ms for the two-domain structure to form. Because the static domain does not precess, the signal from coil *3* rapidly disappears (this coil is located in the large-field region, which is exactly where the SD forms); the HPD forms in the sensitivity region of coil *2*, and the signal from this coil is large in amplitude. Magnetic relaxation leads to a decrease in the HPD size, therefore the amplitude of the signal from coil *2* slowly decreases, the rate of the decrease markedly increasing when the interdomain wall enters the sensitivity region of coil *2*. It should be noted that the duration of the signal shown in Fig. 4a greatly exceeds the characteristic dephasing time for non-interacting spins ($T_2^* \sim 0.7$ ms for the conditions of the experiment).

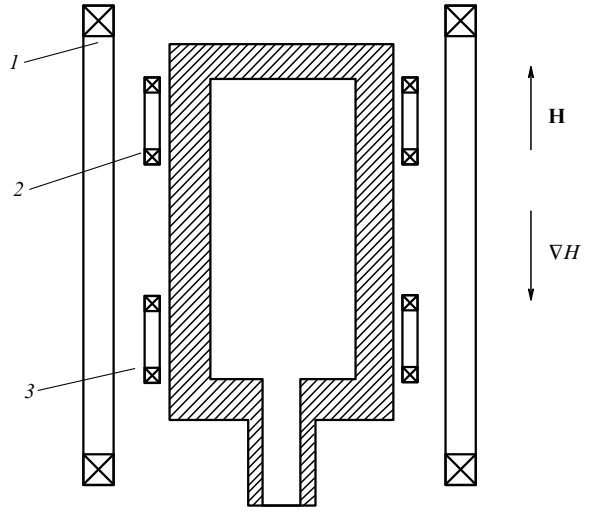

Figure 3. Experimental cell for HPD studies. The experimental volume is 4 mm in diameter and 8 mm in length. All the cells used were made from Stycast-1266 epoxy resin.

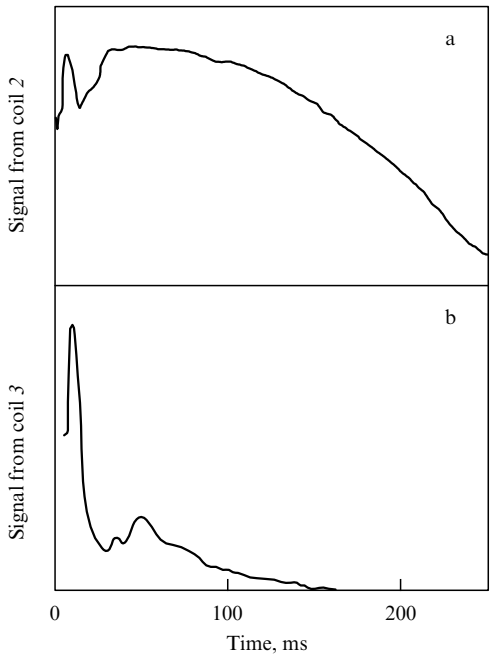

Figure 4. Time dependence of induction signal amplitudes from coil *2* (a) and coil *3* (b). Magnetic field and field gradient directions are as in Fig. 3. $P = 29.3$ bar, $H_0 = 142$ Oe, $\nabla H = 0.1$ Oe cm^{-1}, $T = 0.63T_c$ (where $T_c = 2.43$ mK is the superfluid transition temperature at 29.3 bar).

Predictably, reversing the direction of the field gradient interchanges the roles of the coils: now it is the signal from coil *2* which is found to quickly disappear, whereas that from coil *3* has a large amplitude and is observed to persist for a long time. It turned out that the magnetic relaxation of the two-domain structure also well explains the way in which the frequency of the observed LLIS depends on time. That the magnetization deviation angle in the observed HPD is close to θ_0 was checked by comparing the initial signal amplitude (Fig. 4a) with the initial amplitude of the induction signal in an identical experiment with a normal phase (where the signals from both miniature coils were practically the same and did not depend on the field gradient direction). Addi-

tional experiments confirmed that the magnetization deviation angle in the SD is zero and that it is this fact — rather than spin dephasing in the sensitivity region of coil *3* — which accounts for there being no induction signal in the case of Fig. 4b. The experiment was essentially as follows. During the existence of the HPD, a weak probe pulse was applied to that of the miniature coils in which there was no signal, and then the initial amplitude of the induction signal was compared with that of the signal the same pulse produced when applied to the unperturbed normal phase of ^{3}He.

5. A homogeneously precessing domain under the conditions of continuous wave NMR

The Zeeman energy dissipated in a two-domain structure can be compensated by continuously pumping energy from a transverse, circularly polarized, small-amplitude rf field. In a coordinate system rotating at the frequency of the (x-directed) rf field, the power transfer from the rf field to the nuclear spin system of the HPD is given by

$$W = \int_V h\omega M_y \, \mathrm{d}V = \int_V h\omega |\mathbf{M}| \cos\beta \sin(\alpha - \phi) \, \mathrm{d}V, \quad (10)$$

where h and ϕ are the amplitude and phase of the rf field, respectively. If the amplitude h is sufficiently large, the HPD precession phase α can tune itself to the phase of the rf field in such a way that the power absorbed from the rf field will be equal to that dissipated in the HPD. Then, changing the rf field frequency will correspondingly change the HPD precession frequency and the interdomain wall position, the latter of which is determined, as before, by the condition that the precession frequency be equal to the local Larmor frequency. Experiments showed that an rf field of large enough amplitude (~ 0.01 Oe) makes it possible not only to maintain (and to control the length of) an already existing HPD but also to form the HPD [18]. In practice, it is more convenient to vary H_0, the spatially uniform component of the external magnetic field $H(z) = H_0 - z\nabla H$, than the rf field frequency.

Figure 5 shows the signals of absorption ($\propto \int M_y \, \mathrm{d}V$) and dispersion ($\propto \int M_x \, \mathrm{d}V$) obtained in such an experiment. The cell used was different from that in Fig. 3 both in size (6 mm in both diameter and length) and in having only one receiver-transmitter coil (which covered the entire experimental volume). As H_0 decreases, an HPD forms at $H_0 = H_1$ [the rf field frequency being $gH(z_2)$], and the formation of the interdomain wall and its associated magnetic relaxation due to spin diffusion lead to a rapid increase in absorption. As H_0 decreases still further, the area of the wall remains unchanged and the dissipation does not really increase. There is a (linear) increase in the volume of the HPD, however, which leads to the linear growth of the dispersion signal. At the field value $H_0 = H_2$ the HPD fills the cell completely, and the domain wall disappears (more precisely, its area greatly decreases due to the HPD entering a narrow channel). As a result, the spin diffusion contribution to the magnetic dissipation is drastically reduced, the absorption drops, and the dispersion ceases to grow. Upon further decrease in H_0, the absorption resumes increasing because in the HPD the frequency shift from the local Larmor frequency increases and, accordingly, the Leggett–Takagi relaxation increases in both magnitude and importance. To compensate for this increase in absorption, the precession phase starts changing significantly. The power absorbed from the field reaches a maximum at $\alpha - \phi = \pi/2$,

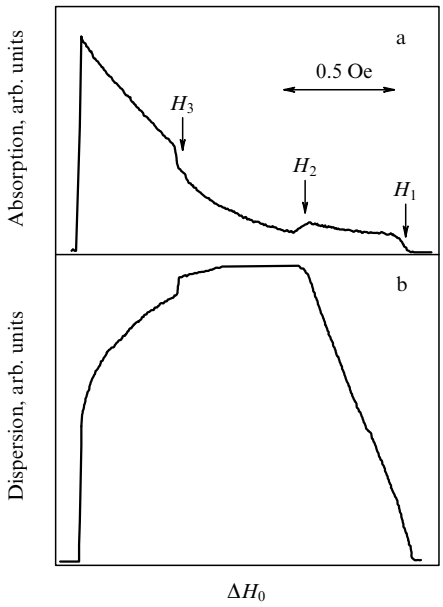

Figure 5. Absorption (a) and dispersions (b) signals for an HPD formed by the continuous wave NMR technique. The magnetic field gradient was directed such that the HPD formed near the upper edge of the cell and filled the entire experimental volume as H_0 decreased. $P = 11$ bar, $H_0 = 142$ Oe, $\nabla H = 0.83$ Oe cm^{-1}, $T = 0.57T_c$.

after which the HPD is destroyed. Note that prior to this destruction, jumps of yet unknown nature are observed in the signals at $H_0 = H_3$. When the field is backscanned after the destruction of the HPD, the two-domain structure does not form, but there are near-standard signals with much smaller amplitudes compared to signals from the HPD. If the scanning of the field is stopped and the continuous rf field turned off before the destruction of the HPD, then an LLIS is observed, as expected.

From expression (10) it follows that when the HPD size (or equivalently, the magnetic dissipation) is held fixed, an increase in h should lead to a decrease in $\alpha - \phi$. In practice, already at $h \gtrsim 0.01$ Oe the difference $\alpha - \phi \ll \alpha$, i.e., the rf field and the precession are practically in phase. This provides the ability to control the HPD precession phase, which proved to be very useful in experiments to study the flow of spin supercurrent through a channel.

6. Flow of spin supercurrent through a channel

The experimental chambers that were used in Refs [19–21] to study the flow of spin supercurrent through a channel consisted of two cells connected by a horizontal channel. Figure 6 shows what the most often used chamber looks like. In both cells, continuous rf fields created by independent receiver-transmitter NMR coils (*1* and *2* in Fig. 6) helped maintain the HPDs. The point to note here is that these HPDs also 'leaked' into the channel, a process which was controlled using miniature pickup coils *3* and *4* on the channel. By varying the rf field phases, a difference in precession phases was created between two HPDs, with rf field amplitudes being large enough to consider that $\Delta\alpha \approx \Delta\phi$. The phase comparison of the signals from coils *3* and *4* revealed that a precession phase gradient developed in the channel. This led to a spin supercurrent in the channel, which transferred the longitudinal magnetization (and hence the Zeeman energy) from one HPD to another. As a result, the rf powers absorbed by the domains changed as compared to the no-spin-current

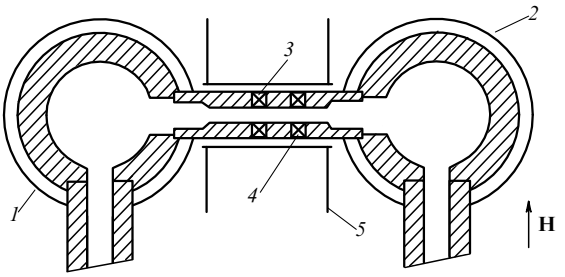

Figure 6. Experimental cell for superfluid spin current studies. The cell consists of two experimental volumes connected by a channel. Both volumes have the form of a cylinder (4.5 mm in diameter and 5 mm in length), whose axis lies in the horizontal plane. The narrow portion of the channel has a diameter of 0.6 mm and a length of 5.5 mm. *1* and *2* are independent receiver-transmitter rf coils, *3* and *4* are miniature pickup coils on the channel, *5* is a copper screen for screening the rf field from coils *1* and *2* in the channel region.

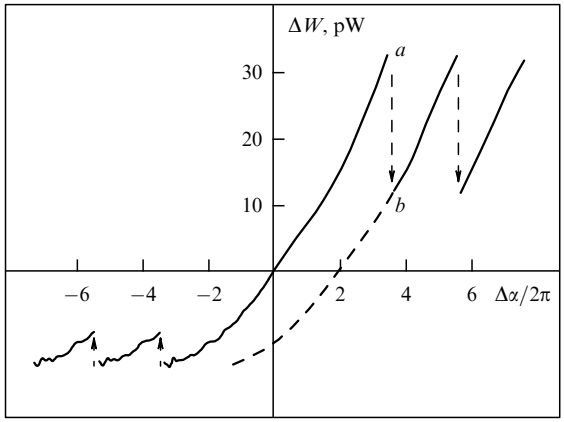

Figure 7. Absorption in one of the HPDs as a function of the precession phase difference between the precessing domains [left (right): $\Delta\alpha$ decreases (increases) from $\Delta\alpha = 0$]. Phase drops are shown by arrows ($a \to b$). If one ceases to increase and starts decreasing the phase difference at point b, the dashed dependence and, later, the phase drops, are obtained. $P = 29.3$ bar, $H_0 = 142$ Oe, $T = 0.48T_c$.

situation: in one of the HPDs the absorption signal decreased, and in the other it increased. By measuring the change in absorption it was possible to determine the current of magnetization. It was found that as the difference in precession phases between the HPDs increased, the current increased to a certain critical value beyond which both the phase gradient and current in the channel exhibited an abrupt drop, and then the above processes repeated themselves in cycles in such a way that the period in the current – $\Delta\alpha$ dependence was always a multiple of 2π (Fig. 7). This is due to the phase slip phenomenon and analogous to the so-called resistive state in superconducting wires. What enables the phase drop to occur is the appearance in the channel of a phase slip center with $\beta = 0$, which makes the phase α indefinite. The magnitude of the critical spin current was obtained theoretically in Ref. [22]. According to theory, the critical value of the spin current is reached when the precession phase gradient is $1/\xi_s$, where the spin correlation length ξ_s is the analog of the Ginzburg – Landau correlation length of superconductivity theory. The spin correlation length depends on the difference between the HPD precession frequency ω and the local Larmor frequency ω_L in the channel,

$$\xi_s = \frac{c}{\sqrt{\omega - \omega_L}} \,. \tag{11}$$

Thus, by varying H_0 (and thereby the local Larmor frequency in the channel), it is possible to vary ξ_s in the course of the experiment (the critical current in such an experiment must be proportional to $\sqrt{\omega - \omega_L}$). Note that the dependence of the current on $\Delta\alpha$ as shown in Fig. 7 is not antisymmetric: the current flowing into the channel is always larger than the current out. The reason is that part of the transferred Zeeman energy serves to compensate the magnetic dissipation in the channel (where the rf field is zero) — with the result that the precession phase gradient varies monotonically along the channel. However, because what is measured experimentally is $\Delta\alpha$, not α, it follows that the measured dependence of the critical current on $\sqrt{\omega - \omega_L}$ should be compared with theoretical estimates that take into account corrections for the magnetic relaxation in the channel. Such a comparison has been made and a good agreement between theory and experiment was found in Ref. [21].

Under realistic experimental conditions, spin correlation length can reach values on the order of 1 mm. Analogy with superconductivity suggests that a sufficiently narrow and short (or a bottlenecked) channel may produce a nonhysteretic current – phase dependence, thus enabling a transition to a Josephson-like regime as found in microscopic (or tunneling) superconducting junctions. Testing this assumption involved using a cell which, unlike that of Fig. 6, had a channel bottleneck 0.3 mm in length and 0.5 mm in diameter. The experiment did reveal a nonhysteretic current – phase dependence [23]. Furthermore, because ξ_s could be varied easily in the course of the experiment, the transition from the Josephson regime to the phase slip regime was observed to occur (at $\xi_s \sim 1$ mm as expected).

The fact that magnetic relaxation violates spin conservation does not run counter to the notion of nondissipative spin supercurrent, which is caused by order parameter phase gradients rather than the difference in pressure or chemical potential. Dissipation leading to the nonconservation of channel current is not due directly to the current but to the non-spin-conserving magnetic relaxation. Spin current in the experiment above is akin to the flow of superfluid ^{3}He which evaporates as it flows in a heated open trough. In this case, the current flowing out of the trough is also less than that flowing into it, and it is the violation of conservation of mass due to evaporation which serves as the analog of magnetic dissipation.

7. Research applications of the HPD

The follow-up research involved the magnetic analogs of phenomena found in 'usual' superfluid systems. One result in this area was the creation and observation of the spin vortex, a magnetic analog of the quantum vortex [24, 25]. Observations were also made of various modes of the spatially nonuniform HPD vibrations, [26] one of which (the so-called twisting mode) is the analog of the fourth sound in ^{4}He. One useful application of the HPD is in the study of the properties of superfluid ^{3}He-B. In particular, the interaction of HPDs with quantum vortices in ^{3}He-B [27, 28] and with the counterflow of the normal and superfluid components [29] was studied using the rotating cryostat at the Helsinki University of Technology, Finland — experiments which

resulted in confidently identifying vortices of different types in measurements of the magnetic-field-induced superfluid density anisotropy in ^{3}He-B. A study of the relaxation of HPDs enabled a systematic measurement of magnetic relaxation parameters [30]. With its property of a spatially uniform order parameter distribution (texture), the homogeneously precessing domain can be effective in studying texture-sensitive phenomena. In particular, the use of the HPD has permitted Leggett frequency measurements in the B-like ^{3}He phase in an aerogel, whose effect on the texture makes standard NMR methods difficult to use for this purpose [31].

8. Conclusion

In summary, the studies reviewed prove the existence of spin supercurrents in ^{3}He-B and demonstrate the analogy between spin superfluidity on the one hand and 'usual' mass superfluidity and superconductivity on the other. As a result, many experiments were explained and new research directions identified. For example, the electric field should play the same role for spin supercurrent that the magnetic field vector-potential does for superconducting electrons. Although very small in magnitude, this effect can in principle be measured. Also of interest might be to conduct research at ultralow temperatures of around 100 μK, where, even though spin supercurrents are clearly important, very long (of the order of an hour) induction signals are observed which the HPD formation model fails to describe [32]. The homogeneously precessing domain was observed not only in ^{3}He-B but also in the B-like phase of ^{3}He in an aerogel — which, in particular, supports interpreting this phase as the analog of the B-phase of the 'usual' bulk ^{3}He as well as opens new possibilities for its study [33].

Dissipationless (reactive) spin currents can exist in other magnetic systems. At sufficiently low temperatures and high magnetic fields, the effective spin diffusion coefficient in Fermi liquids becomes complex, allowing for dissipationless spin currents [34] and thereby leading to a number of phenomena, some of which are analogous to those observed in ^{3}He-B [35, 36]. For example, normal liquid ^{3}He and ^{3}He–^{4}He solutions were observed to exhibit a structure of two oppositely magnetized domains with an in-phase precessing domain wall [37, 38]. In principle, similar phenomena can also occur in magnetically ordered solids. This requires, in addition to the small magnetic relaxation, that the order parameter be degenerate with respect to one of its orientation angles and that the corresponding gradient term be present in the Hamiltonian. Magnetically ordered solid ^{3}He [39] and antiferromagnet $CsNiCl_3$ [40] are candidate materials for such studies.

References

1. Vollhardt D, Wölfle P *The Superfluid Phases of* ^{3}He (London: Taylor & Francis, 1990)
2. Mineev V P *Usp. Fiz. Nauk* **139** 303 (1983) [*Sov. Phys. Usp.* **26** 160 (1983)]
3. Abragam A, Goldman M *Nuclear Magnetism: Order and Disorder* (Oxford: Clarendon Press, 1982) [Translated into Russian (Moscow: Mir, 1984)]
4. Osheroff D D et al. *Phys. Rev. Lett.* **29** 920 (1972)
5. Borovik-Romanov A S, Bunkov Yu M *Sov. Sci. Rev. Sec. A Phys.* **15** 1 (1990)
6. Fomin I A, in *Helium Three* (Modern Problems in Condensed Matter Sciences, Vol. 26, Eds W P Halperin, L P Pitaevskii) (Amsterdam: North-Holland, 1990) p. 609
7. Bunkov Yu M, in *Progress in Low Temperature Physics* Vol. 14 (Ed. W P Halperin) (Amsterdam: Elsevier Sci. Publ., 1995) p. 69
8. Dmitriev V V, Fomin I A *J. Low Temp. Phys.* **135** 361 (2004)
9. Leggett A J *Ann. Phys.* (New York) **85** 11 (1974)
10. Leggett A J, Takagi S *Ann. Phys.* (New York) **106** 79 (1977)
11. Brinkman W F, Smith H *Phys. Lett. A* **53** 43 (1975); Osheroff D D, Corruccini L R, in *Proc. of the 14th Intern. Conf. on Low Temperature Physics, LT-14* Vol. 1 (Eds M Krusius, M Vuorio) (Amsterdam: North-Holland, 1975) p. 100
12. Fomin I A *Zh. Eksp. Teor. Fiz.* **93** 2002 (1987) [*Sov. Phys. JETP* **66** 1142 (1987)]
13. Fomin I A *Pis'ma Zh. Eksp. Teor. Fiz.* **40** 260 (1984) [*JETP Lett.* **40** 1037 (1984)]; *Zh. Eksp. Teor. Fiz.* **88** 2039 (1985) [*Sov. Phys. JETP* **61** 1207 (1985)]
14. Corruccini L R, Osheroff D D *Phys. Rev. B* **17** 126 (1978)
15. Giannetta R W, Smith E N, Lee D M *J. Low Temp. Phys.* **45** 295 (1981)
16. Borovik-Romanov A S et al. *Pis'ma Zh. Eksp. Teor. Fiz.* **40** 256 (1984) [*JETP Lett.* **40** 1033 (1984)]
17. Borovik-Romanov A S et al. *Zh. Eksp. Teor. Fiz.* **88** 2025 (1985) [*Sov. Phys. JETP* **61** 1199 (1985)]
18. Borovik-Romanov A S et al. *Zh. Eksp. Teor. Fiz.* **96** 956 (1989) [*Sov. Phys. JETP* **69** 542 (1989)]
19. Borovik-Romanov A S et al. *Pis'ma Zh. Eksp. Teor. Fiz.* **45** 98 (1987) [*JETP Lett.* **45** 124 (1987)]
20. Borovik-Romanov A S et al. *Jpn. J. Appl. Phys.* **26** 175 (1987)
21. Borovik-Romanov A S et al. *Phys. Rev. Lett.* **62** 1631 (1989)
22. Fomin I A *Pis'ma Zh. Eksp. Teor. Fiz.* **45** 106 (1987) [*JETP Lett.* **45** 135 (1987)]
23. Borovik-Romanov A S et al. *Pis'ma Zh. Eksp. Teor. Fiz.* **47** 400 (1988) [*JETP Lett.* **47** 478 (1988)]
24. Fomin I A *Zh. Eksp. Teor. Fiz.* **94** (11) 112 (1988) [*Sov. Phys. JETP* **67** 1148 (1988)]
25. Borovik-Romanov A S et al. *Physica B* **165 – 166** 649 (1990)
26. Bunkov Yu M, Dmitriev V V, Mukharskii Yu M *Physica B* **178** 196 (1992)
27. Bunkov Yu M, Hakonen P J *J. Low Temp. Phys.* **83** 323 (1991)
28. Kondo Y et al. *Phys. Rev. Lett.* **67** 81 (1991)
29. Korhonen J S et al. *Phys. Rev. B* **46** 13983 (1992)
30. Bunkov Yu M et al. *Phys. Rev. Lett.* **65** 867 (1990)
31. Dmitriev V V et al. *Pis'ma Zh. Eksp. Teor. Fiz.* **79** 612 (2004) [*JETP Lett.* **79** 499 (2004)]
32. Bunkov Yu M et al. *Phys. Rev. Lett.* **69** 3092 (1992)
33. Dmitriev V V et al. *Pis'ma Zh. Eksp. Teor. Fiz.* **76** 371 (2002) [*JETP Lett.* **76** 312 (2002)]
34. Leggett A J, Rice M J *Phys. Rev. Lett.* **20** 586 (1968); Leggett A J *J. Phys. C: Solid State Phys.* **3** 448 (1970)
35. Fomin I A *Physica B* **210** 373 (1995)
36. Dmitriev V V, Fomin I A *Pis'ma Zh. Eksp. Teor. Fiz.* **59** 352 (1994) [*JETP Lett.* **59** 378 (1994)]
37. Dmitriev V V, Zakazov S R, Moroz V V *Pis'ma Zh. Eksp. Teor. Fiz.* **61** 309 (1995) [*JETP Lett.* **61** 324 (1995)]; Dmitriev V V, Moroz V V, Zakazov S R *J. Low Temp. Phys.* **101** 141 (1995)
38. Dmitriev V V et al. *Physica B* **210** 366 (1995)
39. Fomin I A, Shopova D V *Pis'ma Zh. Eksp. Teor. Fiz.* **42** 162 (1985) [*JETP Lett.* **42** 199 (1985)]
40. Mineev V P *Zh. Eksp. Teor. Fiz.* **110** 2211 (1996) [*JETP* **83** 1217 (1996)]

PACS numbers: **75.10. – b**, **75.25. + z**, 75.50.Ee
DOI: 10.1070/PU2005v048n01ABEH002112

New magnetic states in crystals

S S Sosin, L A Prozorova, A I Smirnov

1. Introduction

One of the major types of magnetic interactions in crystals is the exchange interaction, which is usually described by a

Heisenberg Hamiltonian of the form

$$\hat{\mathcal{H}} = J\hat{S}_1\hat{S}_2\,, \qquad (1)$$

where the exchange integral J is determined by the electron shell overlap of interacting ions, and $\hat{S}_1$ and $\hat{S}_2$ are spin operators. The Hamiltonian of the system of many magnetic ions is written as the sum of pair interactions. Depending on the sign of J, the total ground-state spin of the system takes either a maximum ($J < 0$) or minimum ($J > 0$) value. In the former case, the ground state is a ferromagnetic state of the type $|\uparrow\uparrow\ldots\rangle$, which can occur in crystal structures of any dimensionality and symmetry. Various and diverse properties of ferromagnets have been studied intensively throughout the past century.

For the positive exchange integral, the situation is less trivial. First, the classical (so-called Néel) minimum-spin state $|\uparrow\downarrow\uparrow\downarrow\ldots\rangle$ turns out to be not an eigenstate and can therefore only be considered as an approximation. However, for three-dimensional antiferromagnets the deviation of the ground state from this state — zero-point oscillations of the order parameter — manifests itself only in spin reduction form, meaning that the ordered spin component becomes smaller than the total spin of the ions, $\langle S\rangle/S < 1$. Reducing the dimensionality of the system increases the role of the zero oscillations, leading in the case of a one-dimensional spin chain to a completely destroyed long-range magnetic order. The ground state of a spin chain is a singlet one, with the average spin projection vanishing at each site, $\langle S_i^z\rangle = 0$. In spin-1/2 chains antiferromagnetic correlations fall off with a power law and the excitation spectrum has no gap and close to $\mathbf{k} = 0$ is similar to the spin wave spectrum in an ordinary antiferromagnet [1]. For spin-1 chains, the excitation spectrum is separated from the ground state by an exchange gap, $\Delta \sim 0.4J$, and the correlations decrease exponentially [2]. Due to the presence of the gap, magnetic excitations freeze out at low temperatures $T \ll \Delta$, bringing the magnetic heat capacity and susceptibility to zero. Section 2 discusses one interesting consequence of such a state in antiferromagnets.

Another important difference between antiferromagnetic systems and ferromagnets is the possibility of a geometric exchange frustration, i.e., the peculiar arrangement of magnetic ions in the crystal, which prevents the interacting spins from simultaneously aligning antiparallel. As a consequence, a non-collinear spin structure whose ground state energy exceeds that of the collinear magnet (weak frustration) may form and in some cases makes long-range order completely unachievable (strong frustration), allowing a fundamentally new strong-correlated state — the so-called collective paramagnet — which remains disordered to temperatures $T \ll JS^2/k_B$ [3]. Sections 3 and 4 examine some unusual properties of noncollinear (triangular) antiferromagnets and discuss the major thermodynamic consequence the strongly frustrated exchange interaction has for the particular case of a pyrochlore lattice magnet.

2. Impurity-induced magnetic order in a spin-gap magnet

There is a number of spin-gap systems other than quasi-one-dimensional integer spin chains, including ladder structures [4], dimer systems [5], and alternating-exchange chains. In the last case, as a result of the translational crystal symmetry breaking (the doubling of the lattice spacing), the exchange integral of neighboring ions in the chain alternately changes between two values, $J \pm \delta$. Alternating spin chains may be due to crystal structure [6], but they may also spontaneously result from the so-called spin-Peierls transition, which occurs as a consequence of an exchange energy gain due to dimerization [7, 8]. As a result, the excitation spectrum of a spin-1/2 chain acquires a gap whose magnitude depends on the alternation parameter $\Delta \simeq \delta$ [9] and whose presence leads, as in the case of spin-1 chains, to a finite correlation length $\xi \simeq v\hbar/\Delta$. Being stable to small perturbations like anisotropy and interchain exchange interaction, such a state can be artificially destroyed by nonmagnetic doping. Substituting a nonmagnetic ion for a magnetic one breaks up the spin chain and destroys the singlet state, with the result that regions of antiferromagnetically correlated nonzero average spin projections — i.e., regions of local antiferromagnetic order — form near the impurity atoms. We will call such antiferromagnetic regions clusters. Note that these clusters are formed by the spins of the main matrix against the background of a singlet (i.e., nonmagnetic) state. The number of magnetic ions in a cluster is on the order of ξ/a (a is the interatomic spacing), and the absolute value of the average spin projection has a maximum close to the ends of the chain and decreases in the middle. The cluster has nonzero spin and magnetic moment. For spin-Peierls magnets, the formation of clusters with local antiferromagnetic ordering is considered theoretically in Ref. [10]. The appearance of clusters leads to an unusual phenomenon — the impurity induced antiferromagnetic ordering.

This effect was predicted in Ref. [11] and later observed in spin-Peierls [12] and Haldane [13] magnets and in a dimer spin system [14]. The reason why introducing nonmagnetic impurities leads to magnetic order is that the ends of clusters overlap and that clusters in neighboring chains are correlated by a weak interchain coupling. The resulting order parameter appears to be strongly non-uniform.

Impurity-stimulated magnetic order is conveniently studied using the non-organic spin-Peierls magnet $CuGeO_3$, with a spin-Peierls transition temperature of $T_{SP} = 14.5$ K and a low-temperature spin gap of $\Delta(0) \simeq 25$ K [7]. The spin gap opens at the temperature T_{SP} and approaches a maximum value $\Delta(0)$ below 7 K. The magnetic ions Cu^{2+} ($S = 1/2$) can be substituted with, for example, nonmagnetic ions of Zn and Mg. These impurities occupy the sites of the Cu^{2+} ions in the $CuGeO_3$ with a solubility limit of higher than 6%. Thus, one can control the number of breaks introduced to the dimerized spin chain. Contributions from chain breaks to the susceptibility and magnetic resonance signals are clearly visible against the background of the singlet and nonmagnetic matrix.

The magnetic resonance signal at the antiferromagnetic phase transition usually transforms from the paramagnetic resonance signal to an antiferromagnetic resonance (AFMR) signal. While the paramagnetic resonance frequency is determined by the properties of isolated magnetic ions, the AFMR frequency depends on order parameter oscillations. Thus, a phase transition to the ordered state is accompanied by a transformation of the magnetic resonance spectrum. The observation of this transformation allows one to obtain the temperature and other characteristics of the transition. At high enough impurity concentrations (above 3%) impurity ions are a small distance (on the order of the correlation length ξ) apart. For such concentrations, the transition to the antiferromagnetic state in $Cu_{(1-x)}Mg_xGeO_3$ is somewhat analogous to the phase transition in ordinary 3D antiferro-

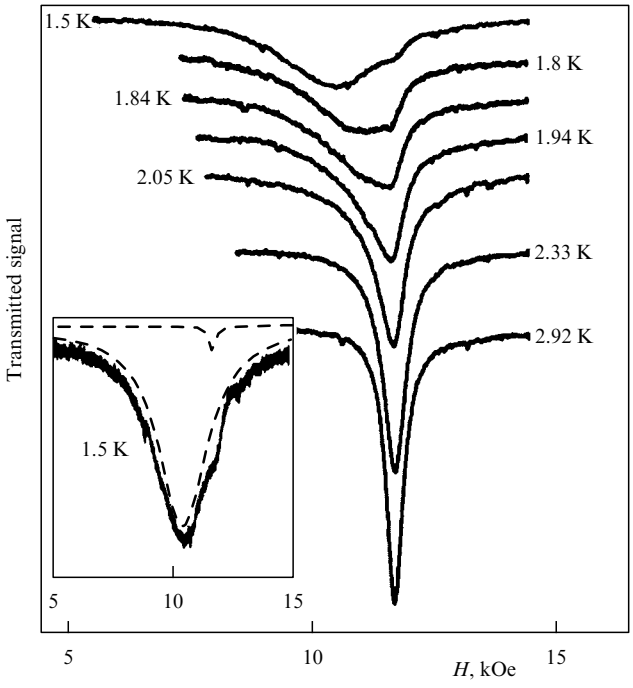

Figure 1. Change in the shape of magnetic resonance line in the vicinity of the Néel temperature in a single crystal of $Cu_{(1-x)}Mg_xGeO_3$: $H \parallel b$, $\nu = 36$ GHz, $T_N = 2.25$ K. Inset shows the expansion of the resonance line at $T = 1.5$ K by two Lorentzian absorptions (dashed lines).

magnets. Of particular interest is the low concentration case, where impurity atoms in a chain are spaced by a distance exceeding the length ξ and spin clusters are separated by remains of the singlet matrix. The process of transition to the antiferromagnetic state as the temperature is decreased was studied in Ref. [15] using the magnetic resonance, a technique which detects both the paramagnetic and antiferromagnetic phases spectroscopically, based on the difference of their resonance frequencies. The experiments were conducted on single crystals of $Cu_{(1-x)}Mg_xGeO_3$ with impurity concentration distributed uniformly to within 10^{-3} over a sample.

Figure 1 follows the evolution of the magnetic resonance spectrum at the transition through the Néel point in doped spin-Peierls magnet $Cu_{(1-x)}Mg_xGeO_3$ with $x = 0.017$. As the temperature decreases, the paramagnetic resonance line splits into two. The first component corresponds to a paramagnetic resonance, the (temperature-independent) resonance field being equal to that of the paramagnetic phase. The resonance field of the second component depends on the temperature, and its frequency-field dependence (see Ref. [15]) corresponds to the spectrum of a biaxial antiferromagnet. There is a wide temperature range where the antiferromagnetic and paramagnetic resonance lines are observed simultaneously. The uniform distribution of impurities over the sample, together with a small transition temperature interval (0.1 K), rule out explaining this coexistence in terms of the macroscopic nonuniformity of the sample. Two simultaneously present resonance modes cannot be explained in the framework of a single-phase examination because order parameter oscillations corresponding to the antiferromagnetic phase rule out the paramagnetic resonance mode and because the paramagnetic phase can even less allow the line to be split. A possible explanation is the macroscopic phase separation of a sample into paramagnetic and antiferromagnetic regions. Let us consider the spin clusters that form around impurity atoms and assume that coherent antiferromagnetic order exists in a region of diameter L^* estimated from the relation

$$k_B T \sim JS^2 \exp\left(-\frac{2L^*}{\xi}\right). \qquad (2)$$

At distances larger than L^* antiferromagnetic correlations are destroyed by thermal fluctuations. The antiferromagnetic correlation distances in transverse directions are determined by corresponding exchange integrals. Then we arrive at a simple model of Ref. [15], with an elliptic-shaped antiferromagnetic region around each impurity center. The length of the ellipse along the chain is estimated from Eqn (2), and its transverse dimension is shorter in proportion to the exchange integral ratio. At high temperature the regions of local antiferromagnetic order are small in size and do not touch one another, long-range order is absent, and the cluster contribution to the susceptibility and the magnetic resonance signal is due to each of the clusters having a total magnetic moment — the reason why the susceptibility and the magnetic resonance frequency have a paramagnetic character. As the temperature is lowered, the clusters increase in size and some of them start touching each other, with the result that more extended regions of coherent antiferromagnetic order — ones containing several impurity atoms — appear. Finally, as shown in Fig. 2, an ordered region stretching throughout the entire sample forms, which corresponds to the percolation threshold for a system of interpenetrating spheres [16]. At and around the percolation value L^* (see Fig. 2) the sample still contains single clusters that are isolated from large antiferromagnetic regions by a weakly perturbed singlet matrix. The free spins of these clusters produce paramagnetic resonance signals in the same way they do above the critical point. Thus, there are three types of regions below the Néel temperature: (1) large enough regions of magnetic order which produce AFMR signals, (2) regions of singlet matrix which have no magnetic response, and (3) single clusters, which are separated from the antiferromagnetic regions by the singlet matrix.

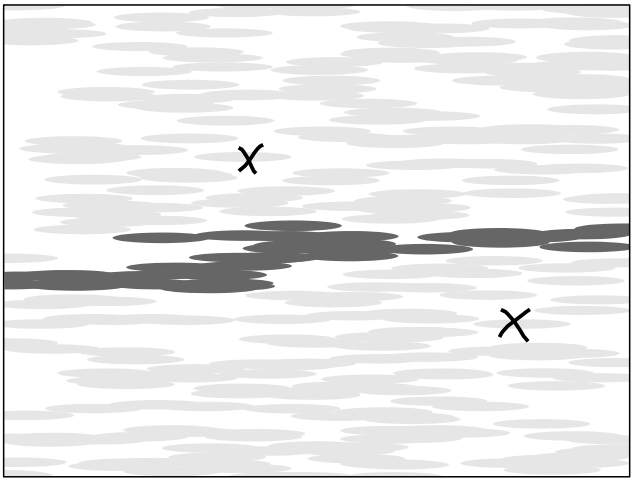

Figure 2. The result of simplified simulation for a structure induced by the impurities of an ordered phase. Grey color indicates the regions of local antiferromagnetic order, black covers the region of macroscopic order, and white corresponds to disordered regions. Two single clusters are marked by crosses.

The obtained picture of microscopic phase separation is in agreement with the results of numerical 2D Monte Carlo simulations for the ground state of spin-Peierls and Haldane systems with impurities [17]. According to this model that takes into account the interchain interaction, the antiferromagnetically correlated spin projections exist in the vicinity of spin vacancies. Away from the impurities the average values of spin projections are close to zero. Importantly, the simulation of Ref. [17] demonstrates a strong, virtually hundred percent, modulation of the order parameter. Assuming that the small order parameter in regions between the impurities will be destroyed by thermal fluctuations at finite temperatures, we conclude that the simulated structure is equivalent to that proposed based on the coexistence of two magnetic resonance signals.

3. Triangular antiferromagnets

As noted in Section 1, the antiferromagnetic exchange interaction, unlike the ferromagnetic interaction, can be frustrated as a result of the structural features of the crystal. A vivid example of this effect is antiferromagnetic structure on a plane hexagonal lattice — the so-called triangular antiferromagnets. Magnetic moments at the vertices of regular triangles cannot form an ordinary collinear structure. The minimum of the classical exchange energy is achieved if the neighboring spins are at an angle of 120° to each other. This is a doubly degenerate state. The antiferromagnetic interaction between planes in real hexagonal crystals does not violate this structure, making spins in neighboring planes align antiparallel. The static and dynamic properties of such systems depend significantly on the ratio of in-plane to interplane exchange interactions between magnetic ions, but in either case differ considerably from the properties of usual two-sublattice antiferromagnets. The largest discrepancies are for the magnetic susceptibility tensors, phase diagrams (especially ones in a magnetic field), and the number and field dependences of the magnetic resonance modes. While the study of quasi-two-dimensional systems has until recently been limited to theoretical work (see, for example, Refs [18, 19]), relatively recently the first experiments — specifically on the compound $RbFe(MoO_4)_2$ — have been made [20]. The most comprehensive review of the magnetostatic and resonant properties of this system is given in Ref. [21].

Quasi-one-dimensional triangular antiferromagnets have been studied extensively over the past two decades, both experimentally and theoretically. Such systems largely occur on crystal structures of the ABX_3-type (where A is an alkali metal, B a magnetic 3d-ion, and X a halogen) which usually belong to the space symmetry group $P6_3/mmc$ (D_{6h}^4). Magnetic ions are located on the sites of a simple hexagonal Bravais lattice, and the exchange interaction between neighbors along the six-fold axis turns out to be 10 to 100 times stronger than the interaction in the basal plane. In the ordered phase neighboring spins along the chains are antiparallel, whereas in the hexagonal planes they are at about 120° to each other. Depending on the sign of the magnetic anisotropy, the planes of the spins can lie either in the basal plane (easy-plane antiferromagnets $CsMnBr_3$, $KNiCl_3$, etc.) or in a plane containing the six-fold axis C_6 (easy-axis antiferromagnets $CsNiCl_3$, $RbNiCl_3$, $CsMnI_3$). Such systems differ widely in their magnetic properties. In this paper, the static and resonant properties of easy-axis structures are described using the example of the compound $RbNiCl_3$. From neutron-scattering experiments [22], at a temperature $T_N \simeq 11$ K this magnet acquires an ordered structure similar to a helicoidal one with wave vector $\mathbf{k} = (4\pi/3a, 0, \pi/c)$, where a and c are lattice parameters. By various estimates, the value of the intrachain exchange interaction is $J \simeq 20$ K [23], and that of the interchain interaction is $J' \simeq 2$ K [26]. The easy-axis anisotropy constant is approximately $D \simeq -0.05$ K. Because $D \ll J, J'$, the triangle exchange structure turns out to be virtually unchanged by relativistic interactions. Due to its quasi-one-dimensional nature, the magnetic structure is strongly influenced by zero-point oscillations, which reduce the average spin on the site to $1.3\mu_B$ at temperatures well below T_N.

Magnetization measurements at a temperature of 1.5 K, carried out with a standard SQUID magnetometer for two magnetic field orientations relative to the easy axis are presented in Fig. 3. Applying a magnetic field perpendicular to the C_6 axis (circles) gives rise to a virtually linear magnetization curve due to the usual canting of the antiferromagnetic sublattices towards the field. But if the field is along the easy axis (in the spin plane), then at $H = H_c \simeq 20$ kOe the curve $M(H)$ exhibits a jump due to the flop of the spin plane (spin-flop-transition). The main difference from the two-sublattice antiferromagnet is that in fields less than H_c a nonzero susceptibility due to the noncollinear structure is observed at $T \ll T_N$. The components of the susceptibility tensor are largely determined by the intrachain exchange interaction. From a simple molecular field calculation, their ratio is $\chi_\parallel = 2\chi_\perp = 1/(8J)$ (where the indices $\parallel$ and $\perp$ are introduced relative to a vector perpendicular to the spin plane). For $RbNiCl_3$ this ratio is $\chi_\parallel/\chi_\perp = 1.8$. The slightly nonlinear high-field magnetization and the different values of the $H \perp C_6$ and $H \parallel C_6$ magnetizations above the spin-flop field are due to the contribution of the zero-point oscillations [27].

The resonance spectra of various easy-axis triangular antiferromagnets have been studied in detail by many researchers [24–26, 29]. In this paper we present the results, similar to those of Ref. [26], of low-temperature spectroscopic measurements performed on a single crystal of $RbNiCl_3$ using a transmission type spectrometer in the frequency range of 30–80 GHz in magnetic field up to 40 kOe. From Fig. 4 it is

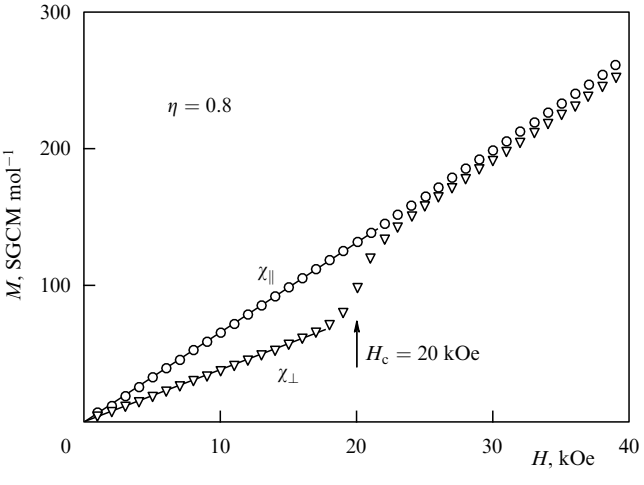

Figure 3. Field dependence of the magnetization of an $RbNiCl_3$ sample at $T = 1.5$ K. Triangles: $H \parallel C_6$, circles: $H \perp C_6$. Solid lines: linear fit for determining $\chi_\parallel$ and $\chi_\perp$. The arrow indicates the spin flop field H_c.

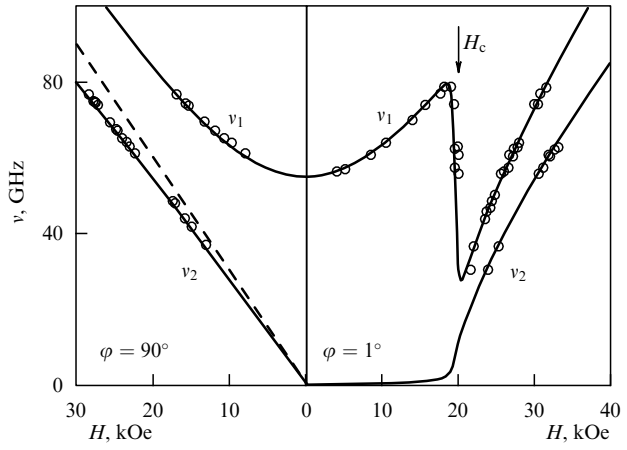

Figure 4. Frequency-field diagrams of an AFMR in $RbNiCl_3$ at $T = 1.3$ K for two magnetic field orientations relative to the C_6 axis. Solid lines are calculated from Eqn (4) with parameters $\eta = 0.8$, $H_c = 20$ kOe as determined from static measurements. The dashed line shows the paramagnetic curve $\nu = \gamma H$. The arrow indicates the value of the field of the spin-flop transition.

seen that for both major magnetic field orientations (φ is the angle between the field and the C_6 axis) the resonance spectrum consists of two branches, labeled ν_1 and ν_2, which have a complex magnetic field dependence. The gap branch ν_1 at $H \parallel C_6$ first increases, then experiences a sharp jump at $H_c = 20$ kOe, and then increases again approaching the paramagnetic dependence. The ν_2 branch remains zero up to H_c, beyond which point it increases in a similar way to ν_1. For the other orientation, both branches increase monotonically, one of them, ν_2, turning out to be close to, but clearly distinct from, the paramagnetic line $\nu = \gamma H$ (where γ is the gyromagnetic ratio).

The resonant properties of such noncollinear structures are extremely hard to analyze in terms of a microscopic spin Hamiltonian and, besides, the presence in a system of many sublattices requires numerous model restrictions to be introduced. The most adequate approach to describe the long-wave part of the resonance spectrum of such structures is to invoke the ideas of exchange symmetry [28]. The spatial spin density of a 120° magnetic structure is specified by the orthogonal unit vectors $\mathbf{l}_1, \mathbf{l}_2$ and the wave vector $\mathbf{k}$,

$$\mathbf{S} \sim \mathbf{l}_1 \cos \mathbf{kr} + \mathbf{l}_2 \sin \mathbf{kr} .$$

The long-wavelength dynamics of a magnet (neglecting its internal degrees of freedom) is specified by the motion of these vectors, and its kinetic energy in a magnetic field is determined by the quadratic form

$$E = \frac{\chi_{\alpha\beta}}{2} (\Omega + H)_\alpha (\Omega + H)_\beta ,$$

where $\chi_{\alpha\beta} = \chi_\perp \delta_{\alpha\beta} + (\chi_\parallel - \chi_\perp) n_\alpha n_\beta$ is the susceptibility tensor of the exchange structure, Ω is the angular rotation velocity in spin space, and $\mathbf{n} = [\mathbf{l}_1 \mathbf{l}_2]$ is the normal vector to the spin plane. For the interaction of the spin system with the crystal (which is weak compared to the exchange), the potential energy is represented, to a first approximation, as a quadratic form in the components $\mathbf{l}_1, \mathbf{l}_2$, which is invariant under the symmetry transformations of the exchange structure. The Lagrangian of the system is then represented in the form

$$\mathcal{L} = E - \frac{\alpha}{2} n_z^2 . \tag{3}$$

For a magnetic field at an arbitrary angle φ to the easy axis, the equilibrium orientation of the spin plane, which is specified by the angle ψ between the vector $\mathbf{n}$ and the easy axis, is determined by

$$\tan 2\psi = \frac{H^2 \sin 2\varphi}{H^2 \cos 2\varphi - H_c^2} ,$$

where $H_c^2 = \alpha/(\chi_\parallel - \chi_\perp)$ is the spin plane flop field for $\mathbf{H}$ along the easy axis ($\varphi = 0$).

Expanding the vectors $\mathbf{n}$ and $\mathbf{\Omega}$ in the Lagrangian (3) to second order in the small off-equilibrium angle θ and varying the resulting expression, we obtain a secular equation for the eigenfrequencies,

$$\begin{vmatrix} \omega^2 - \eta P & i\omega(1-\eta)Z \\ -i\omega(1-\eta)Z & \omega^2 - \eta Q \end{vmatrix} = 0 , \tag{4}$$

where

$$Q = \sqrt{H^4 - 2H^2 H_c^2 \cos 2\varphi + H_c^4} ,$$

$$P = \frac{1}{2}(Q - H_c^2 + H^2) ,$$

$$Z = H \cos(\psi - \varphi) , \qquad \eta = \frac{\chi_\parallel - \chi_\perp}{\chi_\perp} .$$

The first calculation of this type was performed in Ref. [25]. As seen from Eqn (4), as few as two phenomenological parameters, η and H_c, are sufficient to describe the spectrum of an AFMR, the selfconsistency of the approach being emphasized by the fact that these parameters are determined independently from magnetostatic measurements. The results of calculations from Eqn (4) with $\eta = 0.8$, $H_c = 20$ kOe, which are shown by solid lines in Fig. 4, are in excellent agreement with experiment.

Two relativistic branches of the spectrum, ν_1 and ν_2, are associated with the oscillations of the spin plane (vector $\mathbf{n}$) with respect to the crystal and the magnetic field. Clearly, a plane noncollinear structure must also have a third relativistic branch in its spectrum, one associated with the uniform rotations of spins in the plane (about the vector $\mathbf{n}$). If the anisotropic distortion of the triangular structure is small, such a degree of freedom is practically degenerate, making this branch unobservable in $RbNiCl_3$. To describe larger anisotropies, one should introduce the relativistic invariants of higher order in the components $\mathbf{l}_1, \mathbf{l}_2$, which lift the in-plane degeneracy of the spin structure. This was first done to describe the lower branch of the AFMR spectrum in the antiferromagnet $CsMnI_3$ [29] and diamagnetically diluted $RbNi_{1-x}Mg_xCl_3$ [30].

To summarize, the noncollinear magnetic ordering arising due to the weak geometric frustration of exchange interaction in hexagonal crystals has rather unusual properties. The most interesting properties manifest themselves in the long-wavelength spin dynamics, which differs from that in the collinear case in both the type of oscillations and the number of magnetic resonance modes, as well as in their evolution in an external magnetic field. Additional interest in these problems comes from the fact that these effects allow a self-

consistent description in terms of the symmetric 'hydrodynamical' approach which is free of any model restrictions [28].

4. Strongly frustrated ferromagnets

The weakly frustrated exchange interaction considered in Section 3 does not prevent the formation of the Néel state. There exist, however, crystal lattices (such as kagome, garnet, and pyrochlore) whose exchange interaction is not capable of stabilizing any ordering. Over the last decade, several such systems have been investigated [31]. In this paper we limit ourselves to considering the magnetic properties of the pyrochlore antiferromagnet $Gd_2Ti_2O_7$. The magnetic ions Gd^{3+} ($S = 7/2$, $L = 0$) in this crystal form a face-centered cubic Bravais lattice with a regular tetrahedron as a basis (the projection of the lattice on the [111] crystal plane is shown schematically in Fig. 5). The magnetic ground state of such a structure must, in the nearest-neighbor-exchange approximation, satisfy the condition that the total spin on each tetrahedron be zero — but such classical states prove to be infinite in number. The fluctuations between various states that are practically degenerate in energy lead to the consequence that the spin system remains disordered down to $T = 0$ [32, 33]. Heat capacity and magnetic susceptibility measurements [34–36] and neutron experiments [37] have recently shown that $Gd_2Ti_2O_7$ indeed remains disordered over a wide range of temperatures below the Curie–Weiss temperature $\theta_{CW} \simeq 10$ K. The transition to the ordered phase, presumably due to the dipole–dipole interaction, occurs only at a temperature $T_{N1} \approx 1$ K.

The infinite degeneracy of the ground state of a frustrated magnet is equivalent to the existence of a macroscopic number of local soft modes in its excitation spectrum, which corresponds to the rotational degrees of freedom of the spins located at the vertices of the hexagons the edges of the neighboring tetrahedra form in the kagome plane (see Fig. 5). If spins are ordered antiparallel along the perimeter of a hexagon, then in the absence of an external field their rotation through an arbitrary angle in spin space does not change the total exchange energy of the system. Such low-lying modes were observed in the quasi-elastic neutron scattering in $ZnCr_2O_4$, another Heisenberg antiferromagnet on a pyrochlore lattice [38].

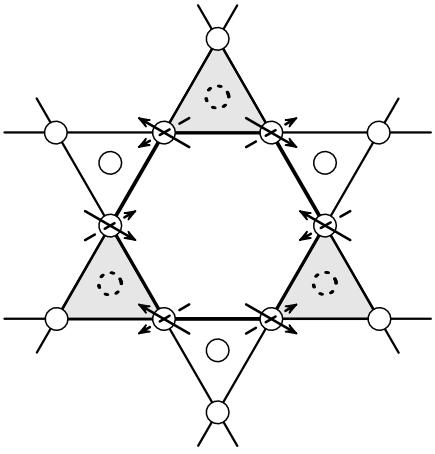

Figure 5. Schematic of the pyrochlore crystal lattice as projected onto the [111] plane. Grey and white triangles indicate, respectively, down- and up-pointing tetrahedra with magnetic ions in their vertices. The solid line traces out the hexagon formed by the faces of the neighboring tetrahedra. The arrows indicate the antiferromagnetic ordering of magnetic moments on the hexagon.

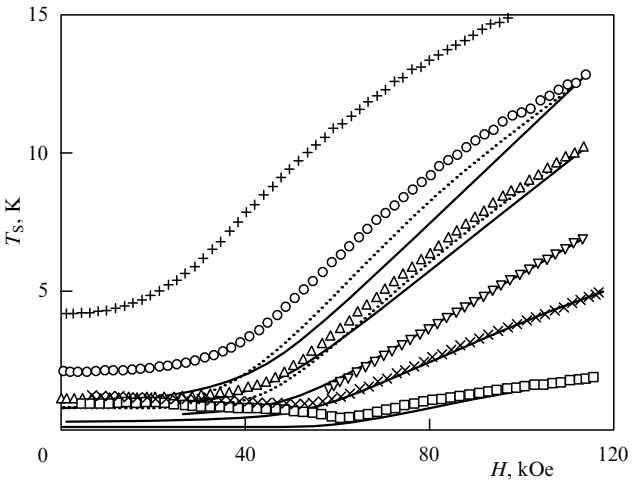

Figure 6. Dependence of the temperature of a $Gd_2Ti_2O_7$ sample on the magnetic field parallel to the [111] plane as the sample is quasi-adiabatically demagnetized from a field of 118 kOe, for various starting temperatures T_i. Solid lines: Monte Carlo simulation, dotted lines: demagnetization curves corrected for the lattice heat capacity.

Thermodynamically, the existence of soft modes manifests itself most importantly in that much of magnetic entropy shows no freeze-out down to well below θ_{CW}. The modes persist up the saturation field H_{sat} (in $Gd_2Ti_2O_7$ $H_{sat} \simeq 70$ kOe) and then acquire a Zeeman gap. The transition from the nondegenerate, fully polarized state that exists above H_{sat} to the infinitely degenerate state below H_{sat} occurs through the 'condensation' of a macroscopic number of local modes and is accompanied by a large change in entropy in the vicinity of the critical field [39]. This property suggests the existence in $Gd_2Ti_2O_7$ of the enhanced magnetocaloric effect which was recently investigated in Ref. [40]. Figure 6 presents the magnetic field dependence of the temperature of a sample of $Gd_2Ti_2O_7$ as it is quasi-adiabatically demagnetized starting from various temperatures T_i. All the $T_S(H)$ lines starting from 10 K and below exhibit a sharp temperature drop in the field range of 120–60 kOe (in contrast to the uniform $T/H = \text{const}$ cooling of an ideal paramagnet), with the maximum value of the initial-to-final temperature ratio T_i/T_f exceeding 10. This experiment clearly demonstrates the fundamental role of strong exchange frustration in the magnetic cooling of $Gd_2Ti_2O_7$. A quantitative description of the obtained data was performed by Monte Carlo simulation of a classical antiferromagnet in the nearest-neighbor approximation (for a detailed description see Ref. [39]). The exchange constant J, the only parameter needed for fitting the simulated to experimental results, can be estimated from the saturation field and the Curie–Weiss temperature, whose values for a pyrochlore magnet, in the molecular field approximation, are given by (see, for example Ref. [39])

$$g\mu_B H_{sat} = 8JS\,, \qquad k_B\theta_{CW} = 2JS(S+1)\,. \tag{5}$$

From either of Eqns (5), $J \simeq 0.3$ K. Solid lines in Fig. 6 present simulation results for this value of J which, taking into account the high-temperature corrections for the lattice heat capacity (as shown dashed) are in excellent agreement

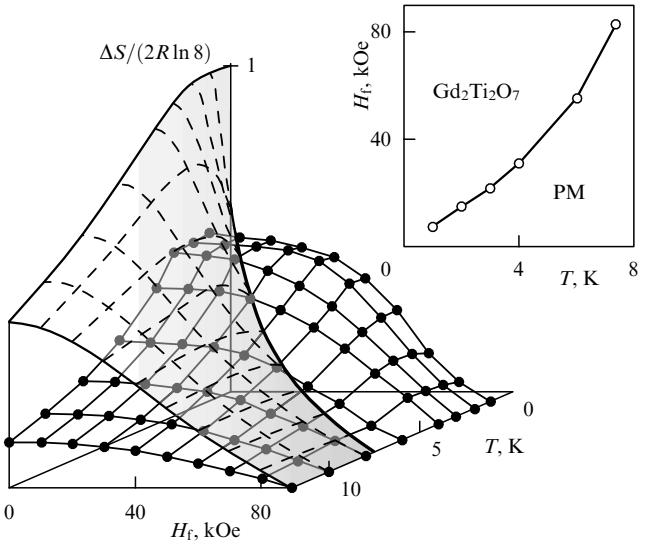

Figure 7. Entropy change in $Gd_2Ti_2O_7$ isothermally demagnetized from $H_i = 90$ kOe, as a function of the final H_f for various temperatures. Grey surface with dashed lines: similar calculations for an ideal spin-7/2 paramagnet. Inset shows the boundary in the $H_f - T$ plane between the regions of preferentially demagnetized pyrochlore and ideal paramagnet (PM).

with experiment — thus directly validating the use of the concept of soft modes in the thermodynamic description of a frustrated magnet.

In concluding this section, we can estimate the cold-productivity of the process based on the adiabatic demagnetization curves $T_S(H)$ given above and using the heat capacity data $C(T)$ for antiferromagnet $Gd_2Ti_2O_7$ obtained with the Quantum Design calorimeter in a strong magnetic field $H = 90$ kOe in the temperature range of 1.5–20 K. For an isothermally demagnetized magnet, the heat it absorbs and its change in entropy are related by the simple relation

$$\Delta Q = T\Delta S\Big|_{H_i}^{H_f}.$$

Let us consider the adiabatic demagnetization curve as it goes from the initial point (H_i, T_i) to the final point (H_f, T_f). Because the entropy remains constant along the curve, the entropy change at a constant temperature T_f and that at a fixed field H_i are related by

$$\Delta S(T_f)\Big|_{H_i}^{H_f} = \Delta S(H_i)\Big|_{T_f}^{T_i} = \int_{T_f}^{T_i} \frac{C(T)}{T}\, dT. \qquad (6)$$

The values of $\Delta S|_T$ calculated from Eqn (6) for demagnetization from the field $H_i = 90$ kOe to the final value H_f at various temperatures are indicated by full circles in Fig. 7 (note that the total entropy of the system remains indefinite). There are two key points to be made here: (1) even at temperatures close to the ordering temperature $T_{N1} = 1$ K the system conserves about half of the total magnetic entropy $2R\ln 8$, and (2) the changes in entropy and heat absorption are a maximum in the strong field region above H_{sat}. This is quite different from the low-temperature behavior of a conventional paramagnet (as shown dashed on the grey surface in Fig. 7), whose entropy is released only at demagnetization down to $H_f \ll H_i$. The $H_f - T$ plot in the inset of Fig. 7 shows the boundary of the region in which the entropy of $Gd_2Ti_2O_7$ changes faster than that of an ideal paramagnet. The cold productivity ΔQ reaches a maximum of 30 J mol^{-1} near 4 K. This amount of heat corresponds to the evaporation heat of a mole of liquid ^{3}He at $T = 3$ K, thus offering the possibility, in principle, of using the pyrochlore magnet $Gd_2Ti_2O_7$ in cryogenic applications.

5. Conclusion

In conclusion, this paper discusses several types of strongly correlated, insulating spin systems with antiferromagnetic exchange interaction in which, unlike conventional magnetic crystals, low-temperature spin order occurs in an unusual way, if at all. In disordered low-temperature structures, new effects, such as magnetic order induced by nonmagnetic impurities, appear. At the critical point for the appearance of this nontrivial ordering, macroscopic phase separation is experimentally observed to occur in the magnetic states of the insulating matrix.

Antiferromagnetic exchange interaction on a hexagonal lattice, if it is geometrically frustrated, can lead to exotic noncollinear triangle magnetic structures with interesting dynamic properties; these properties have been the subject of much study, both experimentally and theoretically. A high level of frustration — such as in a pyrochlore lattice magnet — not only rules out usual ordering but also fully destroys long-range order and leads to a new collective paramagnetic state of the spin liquid type, with unique thermodynamics in a magnetic field. There are prospects for cryogenic applications of the enhanced magnetocaloric effect observed in such systems. Further study of such systems is apparently high on the agenda for the physics of magnetic phenomena.

Acknowledgements. The authors thank V N Glazkov, M E Zhitomirskiĭ, V I Marchenko, and O A Petrenko for their advice and encouragement. The provision of samples by S V Petrov, G Balakrishnan, T Masuda, and K Uchinokura is gratefully acknowledged.

References

1. Bethe H *Z. Phys.* **71** 205 (1931)
2. Haldane F D M *Phys. Rev. Lett.* **50** 1153 (1983)
3. Villain J *Z. Phys. B* **33** 31 (1979)
4. Dagotto E, Rice T M *Science* **271** 618 (1996)
5. Kageyama H et al. *Phys. Rev. Lett.* **82** 3168 (1999)
6. Garrett A W et al. *Phys. Rev. Lett.* **79** 745 (1997)
7. Hase M, Terasaki I, Uchinokura K *Phys. Rev. Lett.* **70** 3651 (1993)
8. Pytte E *Phys. Rev. B* **10** 4637 (1974)
9. Bulaevskiĭ L N *Fiz. Tverd. Tela* **11** 1132 (1969) [*Sov. Phys. Solid State* **11** 921 (1969)]
10. Fukuyama H, Tanimoto T, Saito M *J. Phys. Soc. Jpn.* **65** 1182 (1996)
11. Shender E F, Kivelson S A *Phys. Rev. Lett.* **66** 2384 (1991)
12. Regnault L P et al. *Europhys. Lett.* **32** 579 (1995)
13. Uchiyama Y et al. *Phys. Rev. Lett.* **83** 632 (1999)
14. Oosawa A, Ono T, Tanaka H *Phys. Rev. B* **66** 020405(R) (2002)
15. Glazkov V N et al. *Phys. Rev. B* **65** 144427 (2002)
16. Shante V K S, Kirkpatrick S *Adv. Phys.* **20** 325 (1971)
17. Yasuda C et al. *Phys. Rev. B* **64** 092405 (2001)
18. Chubukov A V, Golosov D I *J. Phys.: Condens. Matter* **3** 69 (1991)
19. Gekht R S, Bondarenko I N *Zh. Eksp. Teor. Fiz.* **111** 627 (1997) [*JETP* **84** 345 (1997)]
20. Inami T, Ajiro Y, Goto T *J. Phys. Soc. Jpn.* **65** 2374 (1996)
21. Svistov L E et al. *Phys. Rev. B* **67** 094434 (2003)
22. Yelon W B, Cox D E *Phys. Rev. B* **6** 204 (1972)
23. Achiwa N *J. Phys. Soc. Jpn.* **27** 561 (1969); Iio K, Hyodo H, Nagata K *J. Phys. Soc. Jpn.* **49** 1336 (1980)
24. Tanaka H et al. *J. Phys. Soc. Jpn.* **57** 1153 (1988)

25. Zaliznyak I A at al. *Pis'ma Zh. Eksp. Teor. Fiz.* **47** 172 (1988) [*JETP Lett.* **47** 211 (1988)]
26. Petrenko O A, Petrov S V, Prozorova L A *Zh. Eksp. Teor. Fiz.* **98** 727 (1990) [*Sov. Phys. JETP* **71** 406 (1990)]
27. Zaliznyak I A *Solid State Commun.* **84** 573 (1992)
28. Andreev A F, Marchenko V I *Usp. Fiz. Nauk* **130** 39 (1980) [*Sov. Phys. Usp.* **23** 21 (1980)]
29. Abarzhi S I et al. *Zh. Eksp. Teor. Fiz.* **104** 3232 (1993) [*JETP* **77** 521 (1993)]
30. Zhitomirskiĭ M E et al. *Zh. Eksp. Teor. Fiz.* **108** 343 (1995) [*JETP* **81** 185 (1995)]
31. Ramirez A P "Geometrical Frustration", in *Handbook of Magnetic Materials* Vol. 13 (Ed. K H J Buschow) (Amsterdam: Elsevier, 2001) p. 423
32. Moessner R, Chalker J T *Phys. Rev. Lett.* **80** 2929 (1998)
33. Canals B, Lacroix C *Phys. Rev. B* **61** 1149 (2000)
34. Raju N P et al. *Phys. Rev. B* **59** 14489 (1999)
35. Ramirez A P et al. *Phys. Rev. Lett.* **89** 067202 (2002)
36. Bonville P et al. *J. Phys.: Condens. Matter* **15** 7777 (2003)
37. Champion J D M et al. *Phys. Rev. B* **64** 140407(R) (2001)
38. Lee S-H et al. *Nature* **418** 856 (2002)
39. Zhitomirsky M E *Phys. Rev. B* **67** 104421 (2003)
40. Sosin S S et al. *Phys. Rev. B* **71** 094413 (2005); cond-mat/0404529